www.czasopisma.pan.pl PAN www.journals.pan.pl
Opto-Electronics Review 25 (2017) 215–221

Contents lists available at ScienceDirect

Opto-Electronics Review

journal homepage: http://www.journals.elsevier.com/opto-electronics review

Performance study of a liquid-core Bragg fiber sensor in presence of a defect layer

R.K. Chourasia, S. Prasad, V. Singh*

Department of Physics, Institute of Science, Banaras Hindu University, Varanasi 221005, India

ARTICLE INFO

Article history:
Received 8 July 2016
Accepted 30 October 2016
Available online 23 July 2017

Keywords:
Bragg fiber based sensor
Liquid filled core
Defect mode
Sensitivity

ABSTRACT

Performance parameter of a Bragg fiber waveguide based resonant sensor in presence of a defect layer in cladding regions is theoretically studied. The Bragg fiber waveguide consists of a liquid-core surrounded by alternate high and low refractive indices materials in cladding regions. Reflectivity of the proposed waveguide based resonant sensor is formulated using transfer matrix method for a non-homogeneous multilayer cylindrical system. The waveguide shows a band gap region with a narrow defect mode in the band gap region under the considered wavelength range. Instead of taking a whole band gap as a sensing signal, here the defect peak is taken as the sensing signal. It is observed that the intensity of defect mode is more sensitive for core refractive index than the intensity of traditional band gap region (lobe). This study shows that the higher sensitivity can be achieved by creating the defect at a position in cladding region where the intensity of transmitted light lies between 40% and 90%. Presence of a defect layer is able to increase the detection accuracy of the sensor and, hence increase the overall performance of this sensor.

1. Introduction

In modern era, multilayered optical waveguides are attracting much interest for applications in biological and chemical sensors due to their high sensitivity and detection accuracy. These multilayer waveguides are also robust, small in size, remote delivery etc. including immunity to electromagnetic interference, intrinsic electrically passivity operations. The working principles of these waveguides are different from the conventional fiber waveguides where the light propagates from one place to other through total internal reflection. The first solid core multilayered optical waveguide was proposed by Yeh et al. [1] with its name Bragg fiber waveguide. The Bragg waveguide consists of a solid core surrounded by high and low periodic refractive indices [2]. The light propagates in solid core through multiple Bragg reflection produced by these periodic arrangements of high and low refractive indices [3]. Since the light propagates in these waveguides through multiple Bragg reflection instead of total internal reflection, therefore it is possible to guide light in low refractive index media that may have small dispersion and propagation losses. During the last decade, the light guidance within media of low refractive index in planar or cylindrical waveguide platforms has been demonstrated for various applications like sensing [4,5], micro fluidic optical interactions [6–8], high power delivery [9,10], particle guidance [11], nonlinear optics [12] and surface-emitting fiber lasers [13]. Also, these multi layered dielectric media have potential applications to high quality-factor cavity-based devices such as radial Bragg resonators [14]. These devices exist today due to the development and improvement of the stringent multilayer fabrication techniques required for these wavelength-scale structures. Terahertz (THz) Bragg fibers can be fabricated with very simple techniques as presented by Dupuis et al. [15]. The alternate layers of polymeric materials can also be suitable candidates for design of low loss Bragg fibers [16].

However, design principles and experimental realization of a Bragg fiber based biosensor through transmittance spectra is demonstrated by Qu et al. [17]. The liquid core Bragg waveguide shows photonic band gap due to its alternate cladding layers [7]. Photonic band gap is a band of wavelengths which is not allowed to propagate through the guiding structure. Researchers used this band gap as a sensing signal in biosensing applications because the position of band gap and transmitted intensity depends on the core refractive index. To enhance the sensitivity by reducing the width of a band gap in a Bragg waveguide based sensor, a low refractive index contrast of alternate cladding materials is used by a group of researchers [17].

* Corresponding author at: Department of Physics, Institute of Science, Banaras Hindu University, Varanasi, 221005 U.P, India.
E-mail addresses: viveks@bhu.ac.in, viveksingh.bhuphysics@gmail.com (V. Singh).

http://dx.doi.org/10.1016/j.opelre.2017.06.002
1230-3402/

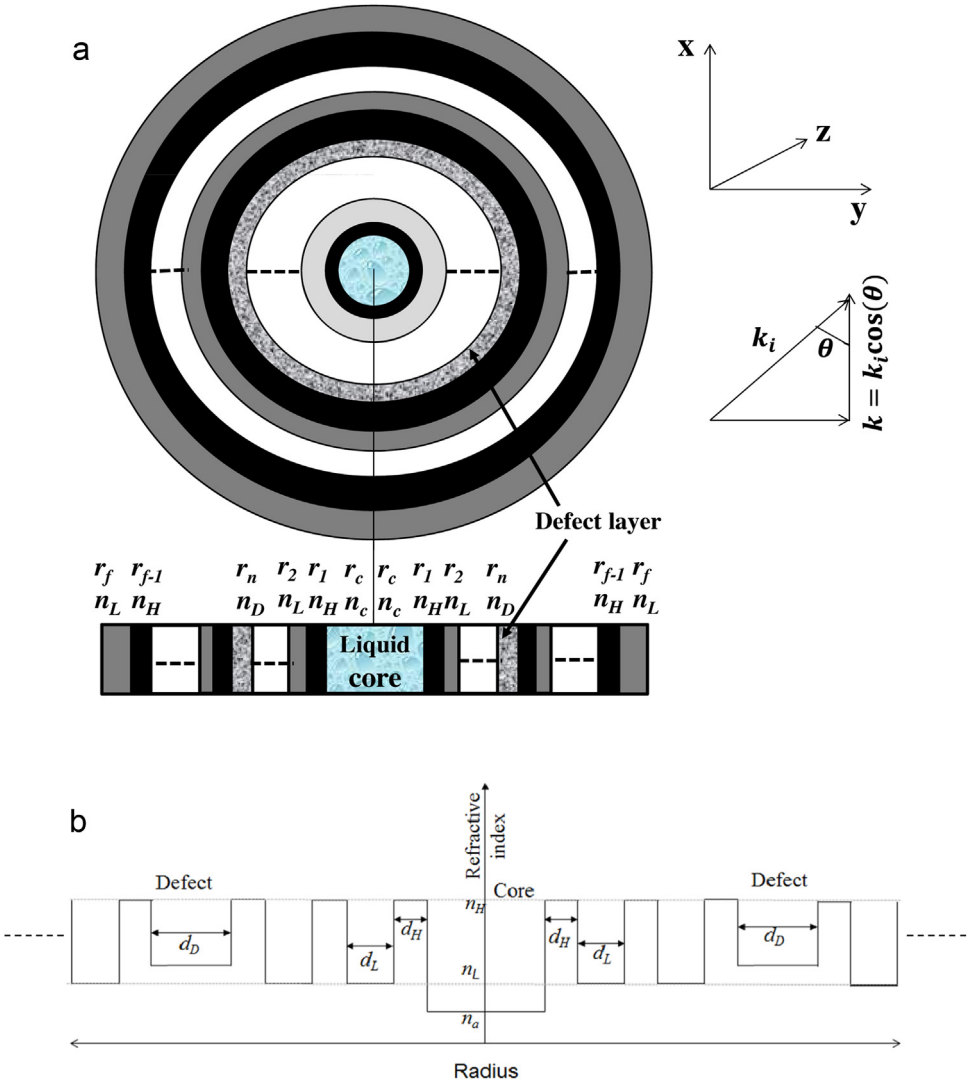

Fig. 1. a) The cross-sectional view of proposed Bragg fiber sensor; b) Refractive index profile of proposed Bragg fiber.

Moreover, presence of a defect layer in alternate periodic layers will provide a defect mode in photonic band gap region [18]. This defect mode is nothing but a narrow transmission bandwidth in the band gap region that can be used as a sensing signal and is the motivation of present work. Also, the presence of defect mode splits the photonic band gap region that may be considered as a reduction of full width at half maxima (FWHM) of band width and able to enhance the overall performance of Bragg waveguide based sensor. Therefore, in the present communication, a defect layer is introduced in a Bragg waveguide by breaking its alternate periodic cladding layers. The paper is organized as follows. In Section 2, basic equations and theoretical formulation of the proposed Braggs sensor is given. The obtained results are discussed and illustrated in Section 3. A conclusion is drawn in Section 4.

2. Theoretical background of the proposed Bragg fiber sensor

2.1. Transfer matrix formalism for homogeneous media in a cylindrical system

The cross sectional view and refractive index profile of proposed Bragg fiber are presented in Fig. 1. Core of the chosen Bragg fiber is filled with liquid and surrounded by high and low polymeric periodic dielectric media. Let chosen polymer materials be non-magnetic layers and their respective refractive indices and thickness are n_H, d_H, n_L, d_L along with defect layer refractive indices and thickness are n_D, d_D. Optical path length of the electromagnetic waves in different periodic layers are supposed to be quarter wavelength and are given by $n_H d_H = n_L d_L = n_D d_D = \lambda_c/4$, where λ_c is the design wavelength of the Bragg fiber. The chosen index profile for the whole Bragg's structure is given as:

$$n(r) = \begin{cases} n_c,\ 0 \le r < r_c; \\ n_H,\ r_c \le r < r_1; \\ n_L,\ r_1 \le r < r_2; \\ \vdots \\ \vdots \\ n_H,\ r_{n-2} \le r < r_{n-}1; \\ n_D,\ r_{n-1} \le r_n; \\ n_H,\ r_n \le r < r_{n+1}; \\ n_L,\ r_{n+1} \le r < r_{n+2}; \\ \vdots \\ \vdots \\ etc. \end{cases} \quad (1)$$

Reflection and transmission response of the Bragg multilayer fiber can be obtained by a cylindrical wave transfer matrix [19]. The Maxwell's equations for a layer having permittivity ε and permeability μ are expressed as [20]:

$$\nabla \times E = -j\omega\mu H, \tag{2}$$

$$\nabla \times H = j\omega\varepsilon E. \tag{3}$$

Considering temporal part of all the fields as exp(jωt), the relation between longitudinal and transvers component of electric and magnetic field is established in the cylindrical coordinate (r, θ, z) system [20]. The Helmholtz wave equations in cylindrical coordinate system are written as:

$$r\frac{\partial}{\partial r}\left(r\frac{\partial H_z}{\partial r}\right) - r^2\frac{1}{\varepsilon}\frac{\partial \varepsilon}{\partial r}\frac{\partial H_z}{\partial r} + \frac{\partial}{\partial \theta}\left(\frac{\partial H_z}{\partial \theta}\right) + \omega^2\mu\varepsilon r^2 H_z = 0, \tag{4}$$

(*For H − polarization*)

$$r\frac{\partial}{\partial r}\left(r\frac{\partial E_z}{\partial r}\right) - r^2\frac{1}{\mu}\frac{\partial \mu}{\partial r}\frac{\partial E_z}{\partial r} + \frac{\partial}{\partial \theta}\left(\frac{\partial E_z}{\partial \theta}\right) + \omega^2\mu\varepsilon r^2 E_z = 0. \tag{5}$$

(*For E − polarization*)

Above equations can be solved using method of separation of variables. Field solution for a cylindrical wave is derived for radial and angular parts [19,21]. The solution for H-polarized wave has three non-zero components (H_z, E_θ, E_r) and they are written as:

$$H_z(r,\theta) = [AJ_m(kr) + BY_m(kr)]e^{jm\theta}, \tag{6a}$$

$$E_\theta = \frac{1}{-j\omega\varepsilon}\frac{\partial H_z(r,\theta)}{\partial r}, \tag{6b}$$

$$E_z = \frac{m}{\omega\varepsilon}\frac{H_z(r,\theta)}{r}, \tag{6c}$$

where J_m and Y_m the are Bessel and Neumann functions, respectively. A and B are the arbitrary constants, $k = \left(\frac{\omega}{c}\right) n$ is the wave vector in a medium, c is the speed of light in free space, and n is the refractive index of that medium. An oblique incidence case on a core cladding interface this wave vector will be the perpendicular component $k = k_i\cos(\theta)$ of the incident wave vector (k_i) as shown in Fig. 1a. The elements of the transfer matrix $\hat{T}$ which correlate the field vector at the initial position r_c to some other point r is determined in Ref. [19] by using Abeles theory dealing with the multilayer structure in Ref. [21] is given by:

$$\hat{T} = \begin{bmatrix} T_{11} & T_{12} \\ T_{21} & T_{22} \end{bmatrix}, \tag{7}$$

$$T_{11} = \frac{\pi}{2}kr_c\left[Y'_m(kr_c)J_m(kr) - J'_m(kr_c)Y_m(kr)\right], \tag{8a}$$

$$T_{21} = j\frac{\pi}{2}kr_c p\left[Y'_m(kr_c)J'_m(kr) - J'_m(kr_c)Y'_m(kr)\right], \tag{8b}$$

$$T_{22} = \frac{\pi}{2}kr_c\left[J_m(kr_c)Y'_m(kr) - Y_m(kr_c)J'_m(kr)\right], \tag{8c}$$

$$T_{12} = -j\frac{\pi}{2}\frac{kr_c}{p}\left[J_m(kr_c)Y_m(kr) - Y_m(kr_c)J_m(kr)\right], \tag{8d}$$

where $p = \sqrt{\frac{\mu}{\varepsilon}}$ is the intrinsic impedance of the medium (p = 377 Ω, for free space). Since main objective of this work is to improve the Bragg's fiber sensor characteristics by creating a defect mode, therefore using above mentioned steps the elements of defect transfer matrix $\hat{T}_D$ are written as:

$$\hat{T}_D = \begin{bmatrix} T_{D11} & T_{D12} \\ T_{D21} & T_{D22} \end{bmatrix}, \tag{9}$$

$$T_{D11} = \frac{\pi}{2}kr_D\left[Y'_m(kr_D)J_m\left(kr'_D\right) - J'_m(kr_D)Y_m\left(kr'_D\right)\right], \tag{10a}$$

$$T_{D21} = j\frac{\pi}{2}kr_D p\left[Y'_m(kr_D)J'_m\left(kr'_D\right) - J'_m(kr_D)Y'_m\left(kr'_D\right)\right], \tag{10b}$$

$$T_{D22} = \frac{\pi}{2}kr_D\left[J_m(kr_D)Y'_m\left(kr'_D\right) - Y_m(kr_D)J'_m\left(kr'_D\right)\right], \tag{10c}$$

$$T_{D12} = -j\frac{\pi}{2}\frac{kr_D}{p}\left[J_m(kr_D)Y_m\left(kr'_D\right) - Y_m(kr_D)J_m\left(kr'_D\right)\right], \tag{10d}$$

where r_D and r'_D are the initial and final position at interfaces of defect layer of the thickness d_D which satisfy the quarter wave stack condition.

2.2. Transfer matrix formalism for a non-homogeneous media multilayer cylindrical system

In previous section, field solution of cylindrical wave, for radial and angular parts in the case of radially homogeneous medium is presented. For a non-homogeneous medium, it is more appropriate to consider the electromagnetic wave as sum of two contrary propagating waves, i.e. superposition of ingoing (converging) and outgoing (diverging) waves. These two cylindrical waves are represented by two Henkel functions. Hence, monochromatic H-polarized outgoing cylindrical wave is further represented as:

$$H_z^+ = AH_m^{(2)}(kr)\exp(jm\theta), \tag{11a}$$

$$E_z^+ = jpAH_m^{(2)'}(kr)\exp(jm\theta), \tag{11b}$$

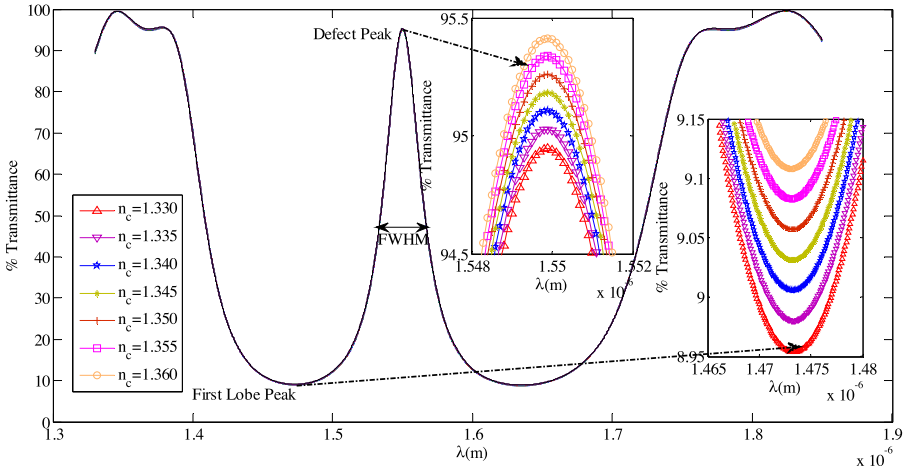

Fig. 2. Percentage transmittance spectra of proposed structure at different core refractive index with fixed defect layer thickness of $1.0d_D$.

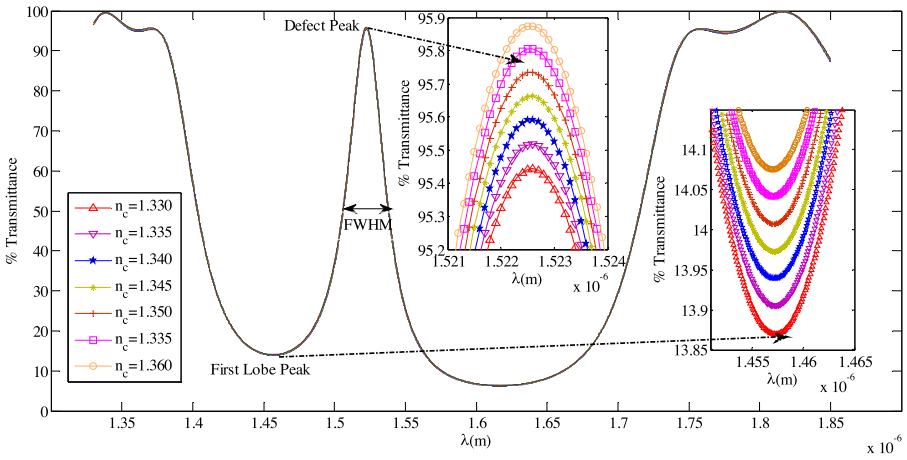

Fig. 3. Percentage transmittance spectra of proposed structure at different core refractive index with fixed defect layer thickness of $0.8d_D$.

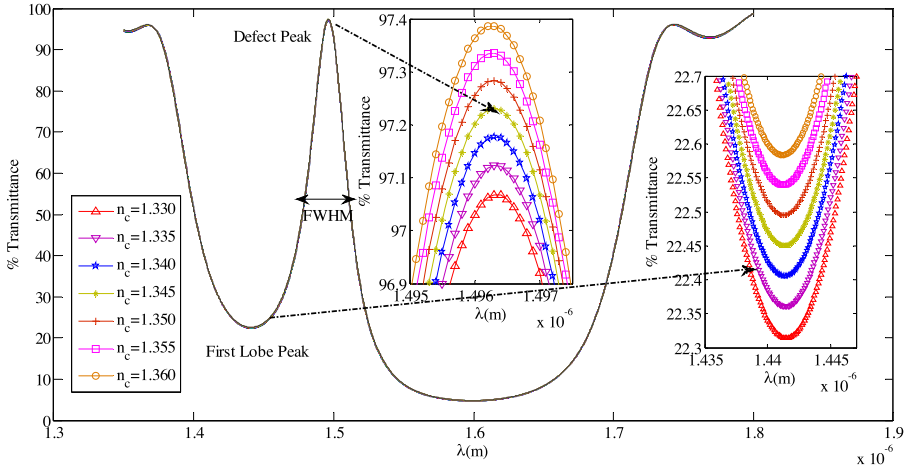

Fig. 4. Percentage transmittance spectra of proposed structure at different core refractive index with fixed defect layer thickness of $0.6d_D$.

and for incoming cylindrical wave is represented as

$$H_z^- = AH_m^{(1)}(kr)\exp(jm\theta), \tag{12a}$$

$$E_z^- = jpAH_m^{(1)'}(kr)\exp(jm\theta), \tag{12b}$$

where $H_m^{(1)}$ and $H_m^{(2)}$ are Henkel function of the first and the second kind, respectively, m is the azimuthal variation of the field, A and B are the arbitrary constant. The field components H_z and E_θ are linear sum of outgoing and ingoing components.

Considering a single layer structure, propagation matrix $\hat{P}$ relating the magnetic field in form of column vector $\left(H_z^+(r), H_z^-(r)\right)$ at r to corresponding column vector at r_0 is given as:

$$\hat{P} = \begin{pmatrix} H_m^{(2)}(kr)/H_m^{(2)}(kr_0) & 0 \\ 0 & H_m^{(1)}(kr)/H_m^{(1)}(kr_0) \end{pmatrix}. \tag{13}$$

Also, the tangential component of fields (H_z, E_θ) at the interface between two layers should be continuous which will generate another matrix, called dynamical matrix $\hat{D}$ as discussed in an usual planar transfer matrix method case [22]. Using dynamical matrix one can develop transmission matrix, $\hat{D}_{21} = \hat{D}_2^{-1}\hat{D}_1$ that connects the amplitudes of waves on two sides of interface. The components of the transmission matrix are:

$$d_{11} = -j\sqrt{\varepsilon_r}\sqrt{\varepsilon_0/\mu_0}\pi/4KrH_m^{(2)}(k_2r)H_m^{(1)}(k_2r)[p_2C_m^{(1)} - p_1C_m^{(2)}], \tag{14a}$$

$$d_{21} = -j\sqrt{\varepsilon_r}\sqrt{\varepsilon_0/\mu_0}\pi/4KrH_m^{(2)}(k_2r)H_m^{(1)}(k_2r)[p_1C_m^{(2)} - p_2C_m^{(2)}], \tag{14b}$$

$$d_{12} = -j\sqrt{\varepsilon_r}\sqrt{\varepsilon_0/\mu_0}\pi/4KrH_m^{(2)}(k_2r)H_m^{(1)}(k_2r)[p_2C_m^{(1)} - p_1C_m^{(1)}], \tag{14c}$$

$$d_{22} = -j\sqrt{\varepsilon_r}\sqrt{\varepsilon_0/\mu_0}\pi/4KrH_m^{(2)}(k_2r)H_m^{(1)}(k_2r)[p_1C_m^{(1)} - p_2C_m^{(2)}], \tag{14d}$$

where K is the wave number of free space.

2.3. Reflectance and transmittance in a multilayer Bragg fiber

Analogous to Fresnel's equation in planar geometry, wave reflection and transmission in multilayer Bragg fiber is obtained using above transfer matrices [19]. The reflection coefficient for multilayer Bragg fiber can be given by:

$$r_d = \frac{(T'_{21} - jp_0c_{m0}^{(2)}T'_{11}) + jp_fc_{mf}^{(2)}(T'_{22} - jp_0c_{m0}^{(2)}T'_{12})}{(-T'_{21} + jp_0c_{m0}^{(1)}T'_{11}) + jp_fc_{mf}^{(2)}(-T'_{22} + jp_0c_{m0}^{(1)}T'_{12})}. \tag{15}$$

Now, reflectance is calculated as $R = |r_d|^2$ and for non- absorbing media, the percentage transmittance is calculated as $T = (1 - R) \times 100$ which values lies between 0% and 100%.

However, sensor sensitivity is defined by the ratio of change in sensor output to the change in physical quantities to be measured. Thus, sensitivity of the Bragg fiber sensor is written as fallowing:

$$S_n = \Delta\%T_{res}/\Delta n_s, \tag{16}$$

where $\Delta\%T_{res}$ is change in percentage resonant transmittance and Δn_s is small change in refractive index of measurend.

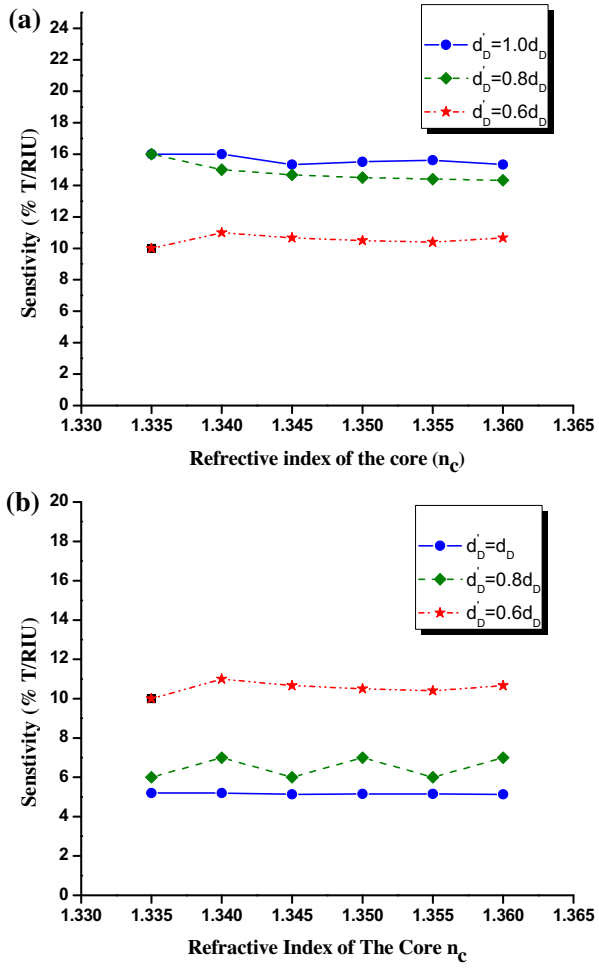

Fig. 5. Variation in sensitivity with core refractive index for (a) defect mode (b) first lobe.

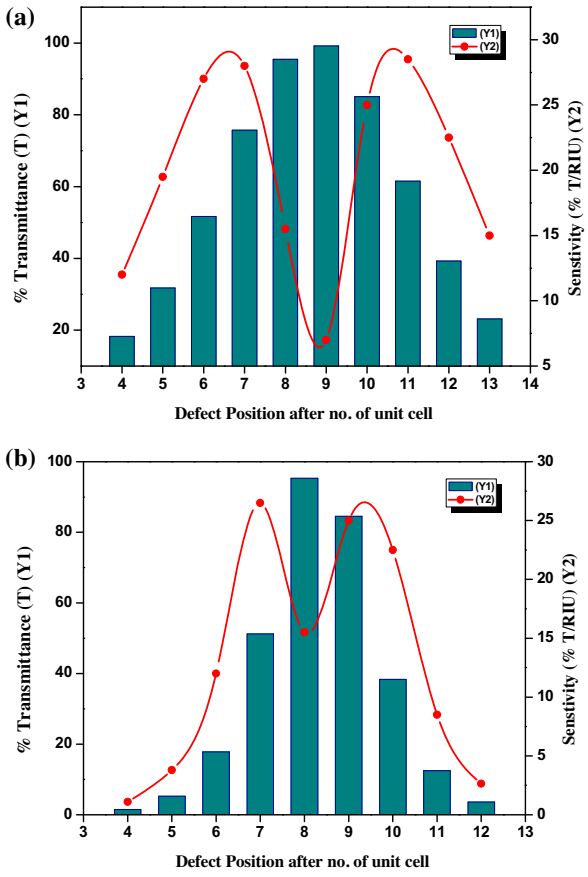

Fig. 6. Variation in transmittance and sensitivity with the position of defect layer in cladding region with cladding refractive index contrast (a) low (b) high.

3. Results and discussion

The proposed Bragg waveguide based sensor is degined for the center wavelength $\lambda_c = 1550$ nm. The Bragg waveguide consists of a liquid filled core of thickness $r_c = 3.78$ μm which is surrounded by 16 unit cell of alternate high and low bilayers claddings having refractive indices $n_H = 1.70$, and $n_L = 1.45$ with their respective thicknesses $d_H = (\lambda_c/4n_H)$ and $d_L = (\lambda_c/4n_L)$. Periodicity of cladding layers are breaked by introducing a defect layer of refractive index $n_D = 1.45$ with thickness $d_D = \lambda_c/4n_D$. Transmission spectra of the proposed resonant sensor is plotted with the help of Eq. (15).

Fig. 2 shows the transmittance spectra of proposed waveguide at different core refractive indices with a fixed width of defect thickness $d_D = \lambda_c/4n_D$. It is clear from figure that a narrow peak of defect mode is obtained at $\lambda_c = 1550$ nm with its FWHM is 31 nm. In present communication, we propose this narrow peak as a sensing signal instead of the first lobe as sensing signal, as proposed by Dupuis et al. [15]. The obtained FWHM of the first lobe is 128 nm. It is clear from inset of Fig. 2 that the intensity of defect mode and the first lobe are varying with change in refractive index of core. This change in intensity occurs due to change in radiation loss of leaky core mode at different core refractive index. For a chosen core refractive index, considered Bragg waveguide structure provides strong optical confinement of leaky core modes and by changing core refractive index, the resonant condition for mode confinement will change hence intensity of transmitted spectra is also change. Figs. 3 and 4 are plotted to see the effect of defect thickness on intensity of transmitted spectra and FWHM for both, defect mode and the first lobe. It is clear from Fig. 3 that as defect layer thickness decreases of $0.8d_D$ the FWHM of defect mode increases of 33 nm while the FWHM of the first lobe 100 nm decreases. Further decrease of defect layer thickness of $0.6d_D$ shows both FWHM of defect mode of 28 nm and the first lobe 86 nm decreases as shown in Fig. 4. The calculated intensity of transmitted spectra at considered defect layer thicknesses are tabulated in Table 1. It is clear from Table 1 that the variation in intensity of transmitted spectra of defect mode is larger than the variation in intensity of transmitted spectra of the first lobe. Hence, obtained sensitivity of defect mode is larger than the obtained sensitivity from the respective lobe. As defect layer thickness decreases, the FWHM of the first lobe decreases hence its overall performance may increase. Therefore, the introduction of defect layer is also able to enhance the overall performance of the first lobe based sensing signal.

Minimum variation in sensitivity with measurend quantity is signature of a good sensor. The variation of sensitivity with core refractive index for both defect mode and the first lobe is shown in Fig. 5. Both cases minimum variation in sensitivity is obtained at defect layer thickness of $0.6d_D$. By comparing Figs. 5a and 5b, minimum variations in sensitivity is obtained for defect mode in comparison with the respective lobe. To obtain maximum intensity of transmitted spectra and sensitivity, the position of defect layer is optimized and shown in Fig. 6. Bar of Fig. 6 shows transmittance and continuous line shows the obtained sensitivity with reference to defect layer position. For low contrast of alternate cladding layers Fig. 6a, larger sensitivity is obtained when the position of defect mode is either in 6th layer, 7th layer or in 9th layer, i.e. just either side of central layer for the considered unit cell (alternate

Table 1
Obtained intensity of transmitted spectra with the variation of refractive index of core at a fixed defect layer thickness.

Core Refractive Index (n_c)	Percentage Transmittance for defect mode (%T)			Percentage Transmittance for first lobe (%T)		
	$1d_D$	$0.8d_D$	$0.6d_D$	$1d_D$	$0.8d_D$	$0.6d_D$
1.330	94.95	95.44	97.07	8.954	13.870	22.310
1.335	95.03	95.52	97.12	8.980	13.900	22.360
1.340	95.11	95.59	97.18	9.006	13.940	22.410
1.345	95.18	95.66	97.23	9.031	13.970	22.450
1.350	95.26	95.73	97.28	9.057	14.010	22.500
1.355	95.34	95.80	97.33	9.083	14.040	22.540
1.360	95.41	95.87	97.39	9.108	14.080	22.590

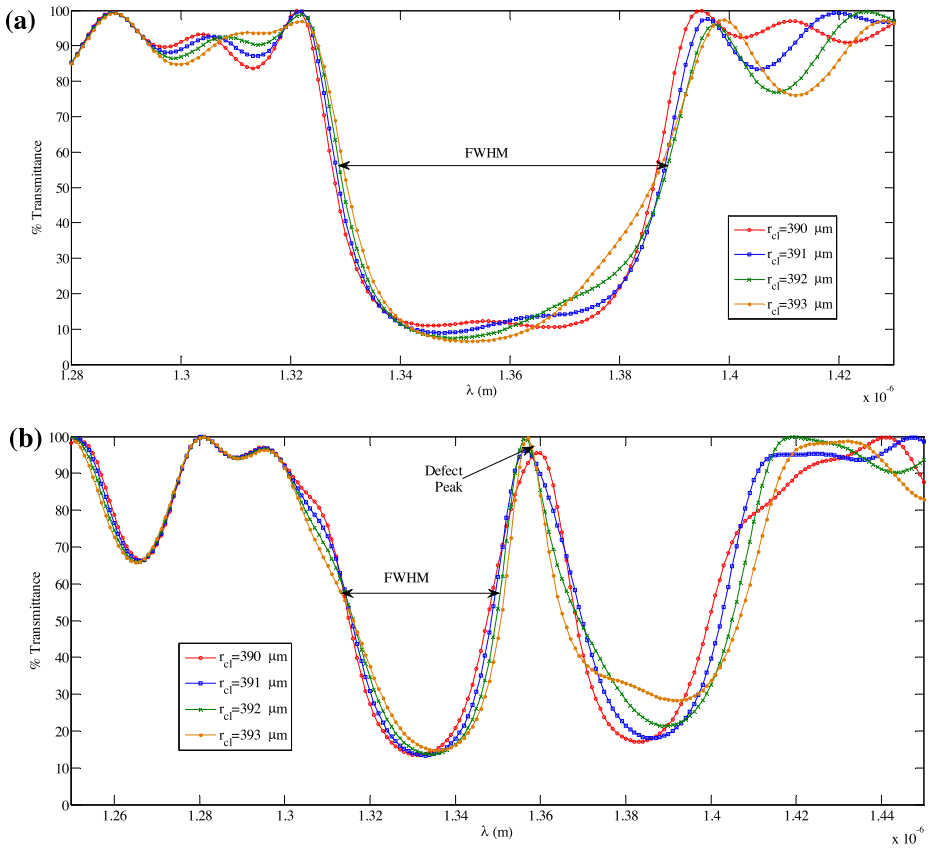

Fig. 7. Spectral shift with variation of core thickness (a) without defect and (b) with defect.

bi-layers) N = 16. In this case, the obtained respective transmittance for 6th, 7th and 10th layer is 51.68%, 75.74%, and 85.06%. It is also clear from this figure that if the transmittance falls below 40% or increased above 90%, then the sensitivity decreases. Similarly, for high contrast of alternate cladding layers Fig. 6b shows that the larger sensitivity is obtained when defect layer position is in 6th, 7th, or in 10th layer. All these cases' transmittance lie from 40% to 90%.

However, the sensing of change in thickness of coated layer in core region as discussed by Qu et al. [17] is further estimated in presence of a defect layer. For comparison point of view the sensitivity, detection accuracy and quality parameter are calculated in both cases, i.e. with a defect layer and without defect layer. The spectral sensitivity in this case can be calculated as $\Delta\lambda_{res}/\Delta r_c$, where Δr_c represents the change in thickness of core coating layer. The detection accuracy describes the degree to which a sensor output represents true value of quantity to be measured and can be calculated as $\Delta\lambda_{res}/\Delta\lambda_{0.5}$, where $\Delta\lambda_{res}$ is the resonant wavelength peak, $\Delta\lambda_{0.5}$ is FWHM of the spectra. Hence, overall performance of sensor in this case is given by $\Delta\lambda_{res}/(\Delta r_c \Delta\lambda_{0.5})$. The spectral change of transmittance at different thickness of the coated layer in core, in absence of defect layer is shown in Fig. 7a. In this figure, r_{cl} shows the remaining part of the core region just after coating by it from sucrose material of refractive index of 1.4418 (@ 60% by weight solution). All the considered design parameters of the Braggs fiber sensor are similar as discussed by Qu et al. [17]. Here, it is found that without defect layer, the maximum sensitivity is of 2.0 nm/μm with FWHM of 58 nm. Fig. 7b shows the spectral change of transmittance at different thickness of the coated layer in core, in presence of defect layer. In this case, obtained maximum sensi-

Table 2
Performance parameter of proposed sensors for monitoring of core thickness.

Sensor parameters	Lobe sensing		Defect mode sensing
	Without defect	With defect	
Spectral sensitivity (nm/μm)	2.0	2.0	1.0
Detection accuracy (D.A.)	0.1379	0.2222	0.3076
Overall quality parameter (μm^{-1})	0.0344	0.0556	0.0769

tivity of the first lobe is of 2.0 nm/μm with FWHM of 36 nm. At this stage, it is clear from Fig. 7 that the presence of a defect layer is able to decrease the FWHM of the lobe without affecting its sensitivity. Hence, overall performance of sensor in presence of a defect layer is increased. The calculated sensitivity, detection accuracy and quality parameters are tabulated in Table 2. In order to see the defect mode performance on the sensitivity, it is clear from Table 2 that although the obtained sensitivity in defect mode case is small of 1.0 nm/μm from the lobe sensitivity but the same time FWHM is also small 13 nm from lobe FWHM, therefore, overall performance in defect sensing case is maximum of 0.0769 in all considered cases.

4. Conclusions

A resonance sensor based on a liquid filled core Bragg fiber waveguide having a defect layer is presented. Required reflectance of this waveguide based sensor is obtained using transfer matrix method. Due to presence of alternate cladding layers, present waveguide shows band gap region. Any break in alternate cladding region is reflected in the form of a narrow transmission band (defect mode) in band gap region. It is observed that the transmittance of this narrow transmission band is more sensitive for change in core refractive index in comparison of the transmittance of band gap. The variation of sensitivity with core refractive index is small in the case of defect mode. Our analysis shows that position of defect mode should not be at the center of alternate cladding region for higher sensitivity. Presence of defect layer able to decrease the FWHM of the lobe without affecting its sensitivity hence overall performance increases. Since FWHM of defect mode is very small in comparison with lobe FWHM, therefore its overall performance is large.

Acknowledgements

The author Ritesh Kumar Chourasia acknowledges to CSIR-HRDG, New Delhi for providing Junior Research Fellowship. The work is also supported by the project No. MRP-MAJOR-ELEC-2013-12554, UGC, New Delhi.

References

[1] P. Yeh, A. Yariv, Bragg reflection waveguides, Opt. Commun. 19 (1976) 427–430.
[2] Y. Prajapati, J.P. Saini, D.S. Chauhan, V. Singh, Effect of Plasma on Modal Dispersion Characteristic of Elliptical Bragg Waveguide, Opt.-Electron. Rev. 22 (1) (2014) 13–20.
[3] P. Yeh, A. Yariv, E. Marom, 'Theory of Bragg fiber, J. Opt. Soc. Am. 68 (1978) 1196–1201.
[4] M. Skorobogatiy, Microstructured and photonic bandgap fibers for applications in the resonant bio- and chemical sensors, J. Sens. 524237 (2009) 1–20.
[5] S. Campopiano, R. Bernini, L. Zeni, P.M. Sarro, Microfluidic sensor based on integrated optical hollow waveguides, Opt. Lett. 29 (2004) 1894–1896.
[6] H. Schmidt, A. Hawkins, Opto fluidic waveguides: I. Concepts and implementations, Microfluid. Nanofluid. 4 (2008) 3–16.
[7] H. Schmidt, A. Hawkins, Optofluidic waveguides: II. Fabrication and structures, Microfluid. Nanofluid. 4 (2008) 17–32.
[8] D. Yin, H. Schmidt, J.P. Barber, E.J. Lunt, A.R. Hawkins, Optical characterization of arch-shaped ARROW waveguides with liquid cores, Opt. Express 13 (2005) 10564–10570.
[9] B. Temelkuran, S.D. Hart, G. Benoit, J.D. Joannopoulos, Y. Fink, Wavelength-scalable hollow optical fibres with large photonic bandgaps for CO_2 laser transmission, Nature 420 (2002) 650–653.
[10] K. Kuriki, O. Shapira, S. Hart, G. Benoit, Y. Kuriki, J. Viens, M. Bayindir, J. Joannopoulos, Y. Fink, Hollow multilayer photonic bandgap fibers for NIR applications, Opt. Express 12 (2004) 1510–1517.
[11] P. Measor, S. Kuhn, E.J. Lunt, B.S. Phillips, A.R. Hawkins, H. Schmidt, Multi-mode mitigation in an optofluidic chip for particle manipulation and sensing, Opt. Express 17 (2009) 24342–24348.
[12] H.T. Bookey, S. Dasgupta, N. Bezawada, B.P. Pal, A. Sysoliatin, J.E. McCarthy, M. Salganskii, V. Khopin, A.K. Kar, Experimental demonstration of spectral broadening in an all-silica Bragg fiber, Opt. Express 17 (2009) 17130–17135.
[13] O. Shapira, K. Kuriki, N.D. Orf, A.F. Abouraddy, G. Benoit, J.F. Viens, A. Rodriguez, M. Ibanescu, J.D. Joannopoulos, Y. Fink, M.M. Brewster, Surface-emitting fiber lasers, Opt. Express 14 (2006) 3929–3935.
[14] J. Scheuer, X. Sun, Radial Bragg resonators, in Photonic Microresonator, Research and Applications, in: I. Chremmos, O. Schwelb, N. Uzunoglu (Eds.), Series in Optical Sciences; Chap. 15, Springer, 2010.
[15] A. Dupuis, K. Stoeffler, B. Ung, C. Dubois, M. Skorobogatiy, Transmission measurements of hollow-core THz Bragg fibers, J. Opt. Soc. Am. B 28 (2011) 896–907.
[16] E. Pone, C. Dubois, N. Guo, Y. Gao, A. Dupuis, F. Boismenu, S. Lacroix, M. Skorobogatiy, Drawing of the hollow all-polymer Bragg fibers, Opt. Express 14 (2006) 5838–5852.
[17] H. Qu, M. Skorobogatiy, Resonant bio- and chemical Sensors using low-refractive-index-contrast liquid-core Bragg fibers, Sens. Actuators B 161 (2012) 261–268.
[18] K.L. Liao, J.J. Wu, T.J. Yang, D. Chen, L. Shen, A Novel Fiber Sensor Based on a Bragg Fiber with a Defect Layer, in: Progress In Electromagnetic Research Symposium, Beijing, China; March 23-27, 2009.
[19] M.A. Kaliteevski, R.A. Abram, V.V. Nikolaev, G.S. Sokolovski, Bragg reflectors for cylindrical waves, J. Mod. Opt. 46 (1999) 875–890.
[20] A.H. Cherin, An introduction to optical fibers, Mc Graw-Hill International, Tokyo, 1983.
[21] M. Born, E. Wolf, Principles of Optics, Cambridge, London, 1999.
[22] P. Yeh, Optical Waves in Layered, Media John Wiley & Sons, Singapore, 1991.